Spectral Ocean Wave Climate Variability Based on Atmospheric Circulation Patterns

ANTONIO ESPEJO, PAULA CAMUS, IÑIGO J. LOSADA, AND FERNANDO J. MÉNDEZ

Environmental Hydraulics Institute "IH Cantabria," Universidad de Cantabria, Cantabria, Spain

(Manuscript received 19 December 2013, in final form 30 April 2014)

ABSTRACT

Traditional approaches for assessing wave climate variability have been broadly focused on aggregated or statistical parameters such as significant wave height, wave energy flux, or mean wave direction. These studies, although revealing the major general modes of wave climate variability and trends, do not take into consideration the complexity of the wind-wave fields. Because ocean waves are the response to both local and remote winds, analyzing the directional full spectra can shed light on atmospheric circulation not only over the immediate ocean region, but also over a broad basin scale. In this work, the authors use a pattern classification approach to explore wave climate variability in the frequency–direction domain. This approach identifies atmospheric circulation patterns of the sea level pressure from the 31-yr long Climate Forecast System Reanalysis (CFSR) and wave spectral patterns of two selected buoys in the North Atlantic, finding one-to-one relations between each synoptic pattern (circulation type) and each spectral wave energy distribution (spectral type). Even in the absence of long-wave records, this method allows for the reconstruction of long-term wave spectra to cover variability at several temporal scales: daily, monthly, seasonal, interannual, decadal, long-term trends, and future climate change projections.

1. Introduction

The surface wave field at any point in a wide basin is the result of the superimposition of the local wind waves and one or more swells propagating from distant sources. As a result, wave spectra often yield two or more wave energy peaks that are commonly ignored when the entire spectrum is treated as one wave system. For this reason, when analyzing wave climate in mixed seas–dominated areas by means of spectral parameters only, some results may be misleading. This lack of information is more evident when dealing with wave statistics or wave climate variability studies.

In recent years, wave spectra characterization has gained considerable relevance as a result of increasing demand for detailed wave information from the marine renewable energy industry. Large efforts have been made in order to offer more comprehensive wave spectrum characteristics, most of them focused on the partitioning of the directional spectrum into components (sea and swell) that physically represent uncorrelated wave systems (Gerling 1992; Wang and Hwang 2001). This approach, although being useful for some specific applications, relies on the ability to tune various adjustable parameters. On the other hand, because the number of peaks in the directional spectrum is not always the same, independent wave system statistics may not correctly define the real picture of the whole ocean wave energy distribution.

Since the 1970s, the synoptic climatology (Barry and Perry 1973) has facilitated the understanding of the local behavior of a wide range of geophysical variables and its relation with synoptic-scale atmospheric circulation patterns. Nowadays, most of the climatic oscillating modes like ENSO, the Arctic Oscillation (AO), and others are obtained by means of principal component analysis (PCA), which is especially useful in reducing the dimensionality of complex spatial patterns like, for example, the sea level pressure (SLP) fields in the North Atlantic (NA). This linear approach assumes that preferred atmospheric circulation states come in pairs, in which anomalies of opposite polarity have the same spatial structure (Hurrell and Deser 2009).

An additional or complementary approach is the cluster analysis, which is a nonlinear multivariate statistical technique that groups together the target spatial fields of a geophysical variable into a small number of

Corresponding author address: Iñigo J. Losada, Environmental Hydraulics Institute, IH Cantabria, Universidad de Cantabria, C/Isabel Torres 15, 39011, Cantabria, Spain.
E-mail: losadai@unican.es

DOI: 10.1175/JPO-D-13-0276.1

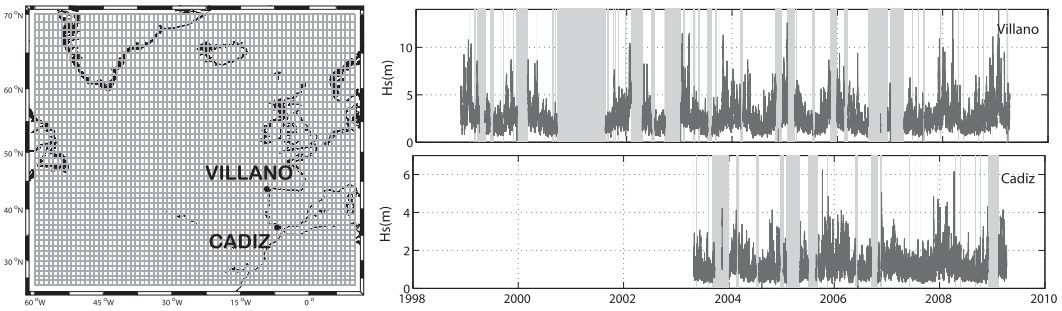

FIG. 1. Locations and H_s time series of the two selected buoys. The CFSR lattice used as a wave predictor is also shown.

representative states or regimes. Several statistical methods have been developed in the field of data mining to efficiently deal with huge amounts of information. These techniques extract features from the data, providing a more compact and manageable representation of some of the important properties contained in the multivariate space (Camus et al. 2011b). Clustering methods have been applied in the field of meteorology identifying atmospheric patterns and deriving relations with local precipitation (Cavazos 2000; Gutierrez et al. 2005), as well as in the field of oceanography in order to select the most representative multivariate sea states for nearshore wave climate characterization (Camus et al. 2011a). Other examples of clustering application can be found in Izaguirre et al. (2012) where by means of the self-organizing maps algorithm, the authors relate extreme wave height anomalies in the NA with certain identified atmospheric situations.

A few studies assessing spectral wave climate variability have been found in the literature, basically because spectral buoy records are not long enough to cover an entire climate period of at least 30 years. Bromirski et al. (2005) used PCA techniques to find SLP modes over the North Pacific, relating these modes to the total energy contained in several frequency bands in selected buoys in the North Pacific (short-period waves, medium, and long period), assuming different spatial origins for each component. Seasonal, interannual, and long-term temporal scales were then addressed, enhancing the effect of El Niño phenomena on the wave spectrum structure in the North Pacific.

Our proposed analysis relies on the directional wave records of two buoys in the eastern NA (Fig. 1) that are the target points for most of the wave energy propagating from west to east in this basin. As these records are not long enough to correctly capture the whole wave climate variability (less than 10 years), we combine clustering techniques looking for recurrent measured wave spectrum types (ST) and circulation types (CT) from the Climate Forecast System Reanalysis (CFSR; Saha et al. 2010), establishing unambiguous relations between them. Once the relations between atmospheric patterns and spectrum types are established, this new method allows reconstructing wave spectra time series during the atmospheric reanalysis temporal domain and thus exploring seasonal to long-term variations of wave energy in the frequency–direction domain. Working with the whole spectrum discloses some nuances of wave climate variability in the NA that would remain hidden if conventional wave statistical analysis based on aggregated parameters were used.

The rest of this paper is organized as follows: In section 2, the buoy data used to characterize spectral wave climate and the SLP fields to find recurrent atmospheric patterns are briefly described. Section 3 presents the proposed methodology to reconstruct long-term time series of directional wave spectra as a result of the combination of buoy and SLP reanalysis data. The spectral wave climate and its climate variability analyses are presented in section 4. Conclusions are given in section 5.

2. Study location and data

Instrumental deep-water buoy spectral data along the northeast (NE) Atlantic have been provided by Puertos del Estado (Spain). Buoys are a Seawatch type that incorporates an accurate three-axis fluxgate compass for buoy orientation measurements. This is important for obtaining high-quality wave directional data (errors below 0.3°). The frequency sensor range is between 2 and 30 s, with errors below 2%. Temporal coverage for the Villano station, located in the northwestern corner of Spain at 386-m depth, spans from 1998 to 2009, while the Cadiz buoy, located close to the Strait of Gibraltar at 450-m depth, starts in 2003. Both provide hourly data to construct the directional full spectra. Time series of the significant wave height H_s determined from the zero-order moment m_0 of the full spectrum as $H_s = 4\sqrt{m_0}$ are shown in Fig. 1. The data available present some gaps (in gray) due to a few periods of different lengths of

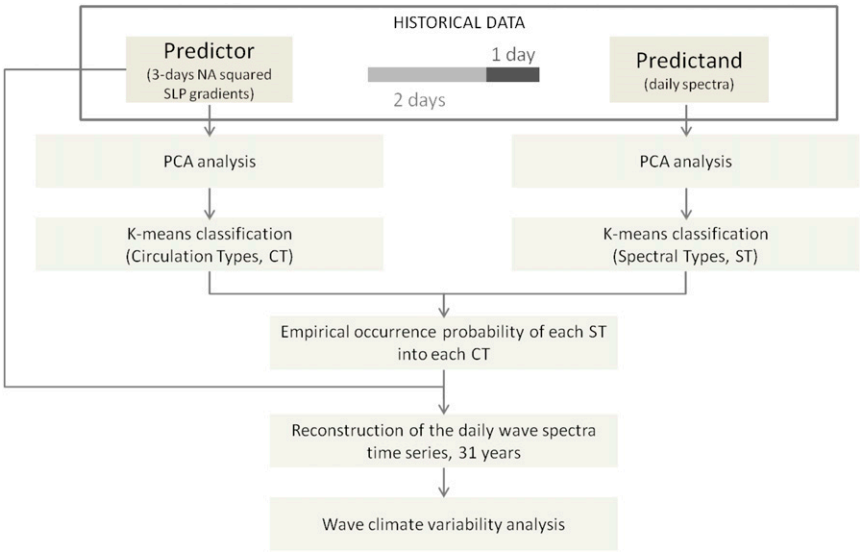

FIG. 2. General framework used to obtain long time series of daily wave spectra.

nonoperation. Nevertheless, each buoy has experienced a number of intense storm events representative of the extreme wave conditions at each location (more than 10 events with $H_s > 10$ m at Villano and $H_s > 4$ m at Cadiz), so it is reasonable to assume that wave climate variability of both the mean and the extreme wave conditions are well captured in these records.

To investigate the synoptic variability of the wave climate and its relation with the atmospheric forcings, the CFSR has been used. This database has been generated by the National Centers for Environmental Prediction (NCEP), covering the 31-yr period from 1979 to 2009. The CFSR was executed as a global, high-resolution, coupled atmosphere–ocean–land surface–sea ice system to provide the best estimate of the state of these coupled domains over this period. All available conventional and satellite observations were included in the CFSR. Output products are available at an hourly time resolution and 0.5° horizontal resolution.

The selected atmospheric forcing area spans from 25° to 70°N and 60°W to 10°E (see Fig. 1) based on the CFSR SLP fields degraded to a $1° \times 1°$ lattice. Selection criteria were based on covering the complete wave generation area of the target points and capturing the most prominent synoptic oscillation modes in the NA, such as the North Atlantic Oscillation (NAO), with blocking or fluid phases, or the east Atlantic Oscillation that characterizes those storms located southwest of the United Kingdom.

3. Methodology

Statistical downscaling methods are based on observed relationships between one large-scale atmospheric circulation pattern of some known variable (predictor: sea surface temperature, geostrophic winds, etc.) and the local behavior of some derived variable (the predictand: rainfall, wave height, etc.). These methods have been broadly applied to wave climate analysis obtaining highly satisfactory results (Wang and Swail 2006; Caires et al. 2006; Camus et al. 2011a; Izaguirre et al. 2012). As a first step, the predictor must be chosen based on physical principles, data availability, and the objective temporal scale to rebuild the predictand. Once the predictor has been selected, the spatial and temporal variability is explored. For this purpose clustering techniques, commonly known as data mining, are useful tools to explore multidimensional spaces. Finally, facing only a number of discrete recurrent states (clusters) of the predictor and by statistically analyzing the predictand values corresponding to each cluster, one-to-one relations between, in our case, the SLP fields in the NA and the full directional spectra at the two study sites can be established. Figure 2 shows the general framework used in this work. Further explanation of the method is conducted in the following sections.

a. Building the predictor

Although the surface marine wind is the driving force of waves, the SLP fields are the variable commonly used when relating ocean waves with synoptic atmospheric states. Moreover, SLP is dynamically related to wind, containing information about wind speed (spacing of the isobars) and direction (orientation of the isobars). Because the swell traveling times in the NA are about 3 days (Alves 2006), a 72-h lag is assumed when relating waves at the target points and the previous 3-day

atmosphere circulation. To more effectively differentiate synoptic atmospheric maps based on the wind speed field and its spatial pattern, the squared SLP gradients are used instead the SLP values (Wang et al. 2012). The squared SLP gradients are determined at each point from the values of the four nearest grid points using the weights proportional to the inverse of the distance. The squared SLP gradient anomalies are determined next by subtracting the baseline climatology of the entire reanalysis period (1979–2009). The resulting high-dimensional fields are defined by 71 × 46 grid points. Therefore, a principal component analysis is applied to eliminate data dependency and redundancy with the minimum loss of variance. PCA finds the minimum d linearly empirical orthogonal functions (EOFs), so that the transformation of the original data explains the maximum variance of the whole multidimensional data space (see Preisendorfer 1988). The reduction of the dimensionality is achieved by creating a new set of orthogonal and ordered variables, the principal components [PCs(t)], which, when multiplied by the d EOFs (or spatial patterns), produce any of the 3-day squared SLP gradients of the original data space.

To find representative patterns of synoptic climatology, the k-means clustering algorithm has been selected. Clustering methods provide a complementary nonlinear alternative to the more frequently used linear methods such as PCA, with the main advantage of handling nonlinear relationships. Besides, it supports the development of synoptic climatologies with an arbitrary number of smoothly transitioning atmospheric states, becoming a powerful tool to provide an easy interpretation of the results by visual inspection.

The k-means clustering technique divides the high-dimensional data space (in our case the PCs vectors) into a number of clusters, each one defined by a prototype and formed by the data for which the prototype is the nearest (Hastie et al. 2001). Given a database of n-dimensional vectors $\mathbf{X} = \{\mathbf{x}_1, \mathbf{x}_2, \ldots, \mathbf{x}_N\}$, where N is the total amount of data (in our case $N = 10\,958$ days) and n is the dimension of each vector $\mathbf{x}_k = \{\mathbf{x}_{1k}, \ldots, \mathbf{x}_{nk}\}$ ($n = 47$ PCs needed to explain the 95% of the variance), k means is applied to obtain M groups defined by a prototype or centroid $v_k = \{v_{1k}, \ldots, v_{nk}\}$ of the same dimension of the original data, where $k = 1, \ldots, M$.

In this case, to facilitate the example, we have considered $M = 25$ clusters or circulation types to characterize the climate variability in the NA (see Fig. 3). In each one of the maps, colors indicate the squared SLP anomalies in pascals squared per meter (related to the wind speed) with the isobars superimposed. As can be observed, this clustering algorithm identifies 25 synoptic types spanning from relative stable atmospheric states with high pressure dominance (in the lower-right corner of the lattice) to the most energetic situations with extremely deep lows centered over different parts of the NA. A further analysis reveals the existence of well-known climate regimes such as the fluid phase of +NAO (CT 6) (see Hurrell and Deser 2009). Moreover, different nuances with remarkable effects on waves of the +NAO are displayed in the lattice, which demonstrates nonlinearities in the NAO variability. Note the asymmetries of several possible +NAO states, exhibiting different orientation of the isobars between CT 1, CT 2, and CT 3. In contrast, strong anticyclonic ridges are also displayed: the blocking phase in CT 18 or the Atlantic Ridge in CT 20 (see Cassou et al. 2004). As mentioned before, the most striking advantage of working with squared SLP gradients rather than with SLP is that the classification is focused on exploring spatial wind patterns that are more directly linked with waves than SLP fields themselves. The number of selected clusters dictates how much intracluster variability is explained. Increasing the range of patterns produces a wider range of atmospheric situations that may be important at the local scale. A sensitivity analysis has been undertaken to propose a number of classes. Although better results are obtained when increasing the number of clusters (more intermediate atmospheric states appear), large lattices make the methodology more cumbersome to describe.

According to the representative centroid of each 3-day SLP field, the probability of occurrence of each CT can be determined. Similarly, using the corresponding SLP dates within each cluster, the predictand values can be projected into the CT lattice. Thus, for each CT, the average value (or some desired percentile) of the predictand can be determined. This facilitates establishing relationships between the CTs and the frequency–direction wave energy distribution.

b. *Clustering the wave spectra*

Although H_s is the most common parameter used to describe wave climate variability, wave spectral density provides significantly more information, making it possible to differentiate between distant and local wave generation areas. Variations in the wave energy at a target point depend on the location, fetch parameters, wind speed and direction, and deep-water wave propagation processes. Because long-period waves are only generated by high sustained winds over a large fetch, the behavior of the energy contained in these low frequencies gives an idea about the extreme storm characteristics (Bromirski et al. 2005). On the other hand, because short-period waves experience a more rapid reduction of the wave height (Janssen and Viterbo 1996), the

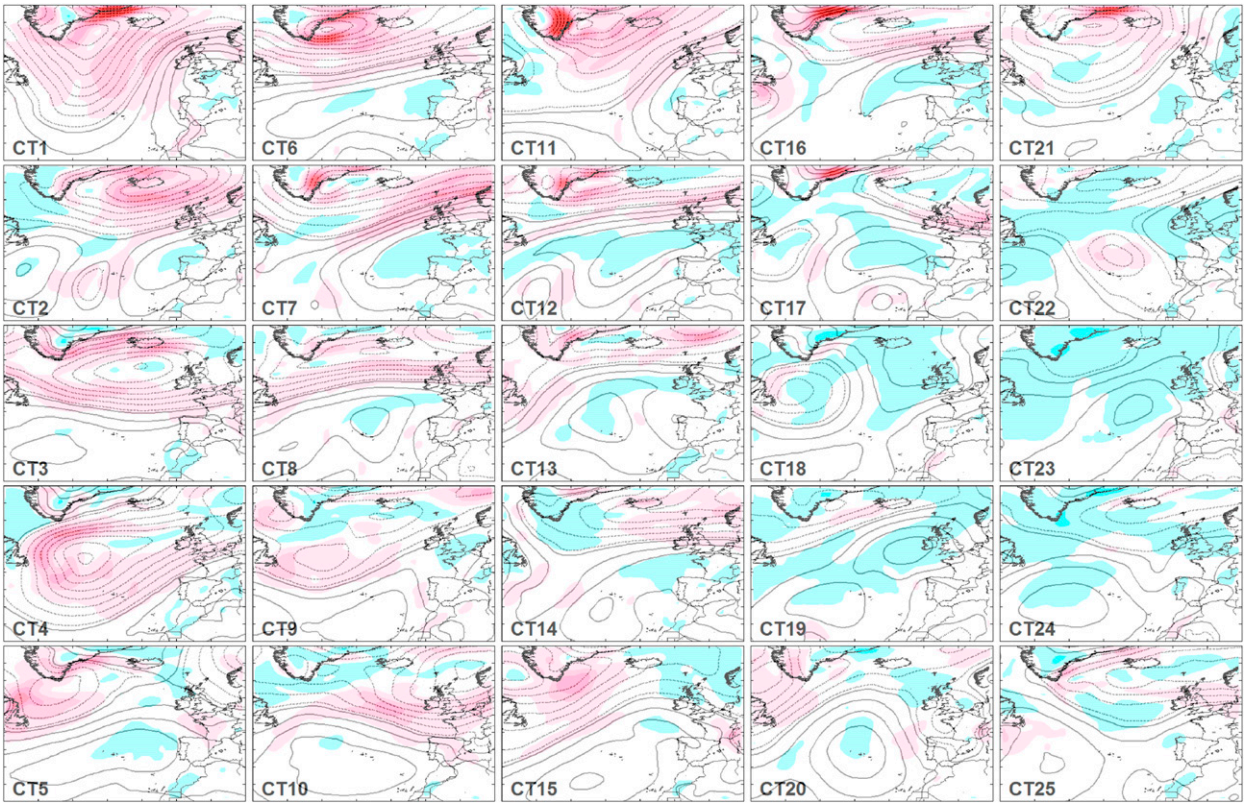

FIG. 3. Circulation-type lattice determined with the 3-day squared SLP gradient anomalies from CFSR between 1979 and 2009. Contours represent isobars while the red–blue color shadings indicate positive–negative anomalies of the squared SLP gradients.

behavior of the energy traveling in these high frequencies provides information about local or regional storms. Supported on this principle, the directional spectrum is discretized in four frequency intervals (from 2 to 5, 5 to 10, 10 to 15, and >15 s) and 22.5° directional intervals. Wave energy contained within each frequency direction is expressed in terms of equivalent significant wave height as $h_{i,j} = 4\sqrt{m_{0i,j}}$, with $m_{0i,j} = \int_{f_i}^{f_{i+1}} \int_{\theta_j}^{\theta_{j+1}} \overline{S(f,\theta)}\, df\, d\theta$, where $\overline{S(f,\theta)}$ is the average daily wave spectrum and $H_s^2 = \sum_i \sum_j h_{i,j}^2$. Although this discretization seems to be appropriate for a good description of the NA wave climate, it should be tuned for capturing major wave climate features at other sites. Figure 4 displays the discretization scheme and an example of a typical mixed sea state from the Cadiz buoy. In this case, wave parameters obtained from this mixed wave spectrum are misleading, especially the wave mean direction that indicates waves coming from the south, when in fact there are two well differentiated wave systems, one young sea from the southeast (SE) and another more developed swell from the west (W). These details show the relevance of exploring the full directional spectrum rather than the wave parameters to better assess wave climate variability.

With this procedure two remarkable facts are determined. First, the wave energy density is not normally distributed, especially in these frequencies and directions where there is no energy throughout most of the time. When the wave spectrum is grouped by bins or packages, the wave energy distribution becomes Gaussian, which is a precondition when a PCA analysis is conducted. Second, results are more easily interpretable by visual inspection in terms of binned wave heights than in the original energetic units.

Following the same procedure as in section 3a, a wave spectral-type analysis has been carried out for the two buoys. Although the *k*-means algorithm has been previously applied in order to classify a number of sea states to relate its occurrence with climate variability indices (Le Cozannet et al. 2011), it has also been applied to a number of aggregated wave parameters. Nevertheless, in this work we have considered the spectrum as a spatial grid of 16 directions and 4 periods, performing the classification with 4 × 16 values and conserving the information about the spectrum structure. Figure 5 displays the 5 × 5 lattice of the discrete spectra obtained from the Villano buoy record (1998–2009); colors indicate the $h_{i,j}$ (cm). The Villano buoy is located in the

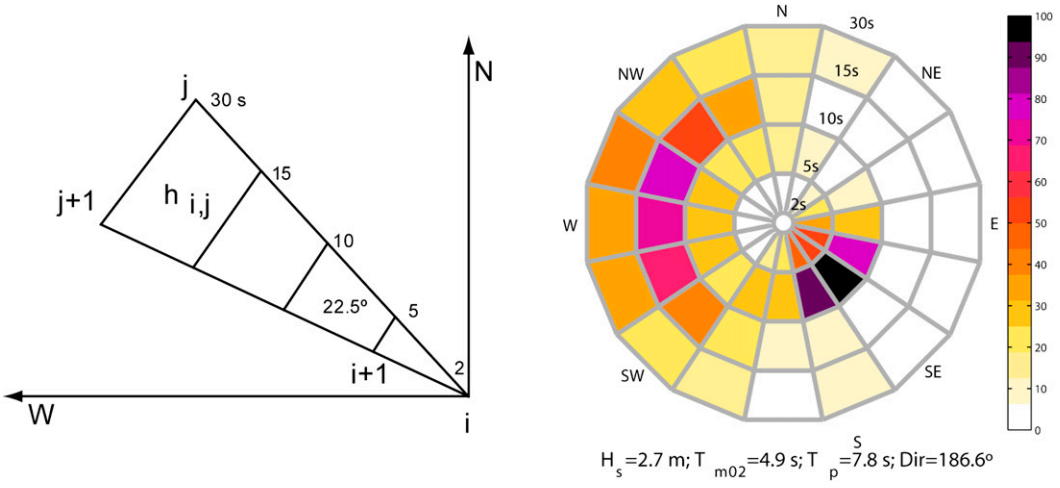

FIG. 4. (left) Wave spectrum discretization scheme and (right) an example of the discretized spectrum (cm) corresponding to a mixed swell and sea at the Cadiz buoy. Directions are expressed following nautical convection (0° indicates waves coming from the north, 90° from the east).

most northwestern corner of the Iberia Peninsula, so it is exposed to almost all the possible wave fields in the NA. The wave spectra respond with northeasterly short-period waves under anticyclone dominant periods over the Bay of Biscay and with long-period swells under active storm periods in the NA. As expected, the classification sweeps a wide range of wave conditions. From the most extreme or energetic sea states (lower-right corner) with significant wave heights above 10 m and large amounts of energy traveling on periods over 15 s to almost flat conditions (upper-left corner) with $H_s < 0.3$ m and $T_p < 10$ s. Moreover, pure swells (ST 18) and mixed sea states (ST 21) are also identifiable. In the case of the ST 21, a remarkable amount of energy from the northeast sector (wind seas with periods below 10 s) is combined with a moderate swell from the northwest (NW) (with periods over 10 s). Another example is the ST 15, in this case resembling one distant swell from the NW and a closer one from the southwest (SW).

Figure 6 shows the STs determined from the Cadiz buoy record. Waves in this region are deeply governed by the Strait of Gibraltar configuration and the relatively sheltered effect from the northwesterly swells produced by the San Vicente Cape in Portugal. As can be seen, waves in this area tend to be smaller, so most of the ST significant wave heights are below 1 m. Another interesting feature is that wave directionality is confined to a narrow distribution. NW swells are transformed into westerlies due to land shadow, and easterly winds manifest their wave energy in the east-southeast (ESE) direction. Again, pure swells (ST 18), wind seas (ST 12) and mixed seas (ST 15 and ST 19) are recognized by the *k*-means algorithm. Even so, those waves coming from the southwest generated by rare storms that used to travel on anomalous southerly tracks in the NA are also detected (ST 25).

c. *Probabilistic relationships between predictor and predictand*

In this section the establishment of the connections between the CTs and the STs at the two studied sites is performed. First, regarding the corresponding CTs dates, the STs are identified. Note that a 3-day lag is used when relating waves and atmospheric patterns (see Alves 2006). For each CT, the occurrence probability of each SP is determined, obtaining a multi-lattice as shown in Fig. 7 for the Villano site. This graphical representation is composed of 5×5 subgrids corresponding to the CT lattice structure. Each subgrid represents the occurrence probability of each ST into each CT. Thus, one can see how CT 4, exhibiting a deep and large low located southwest of Iceland, is expected to produce ($P = 20\%$) the ST 10, which indicates high energetic waves on the longest periods from the west-northwest (WNW) sector and a strong action of the local west-southwest (WSW) winds, transposing energy to the short-period waves in the WSW sector. In the same manner, the most energetic selected wave conditions, ST 25, is related to CT 1 in which the maximum dimensions of the effective fetch in the NA is reached. The same procedure has been followed to determine occurrence probabilities of the STs at Cadiz (not shown here).

It is worthwhile to point out that this work is focused on exploring wave climate variability rather than extreme waves. Thus, although a 5×5 classification seems to be appropriate for this purpose, it is expected to

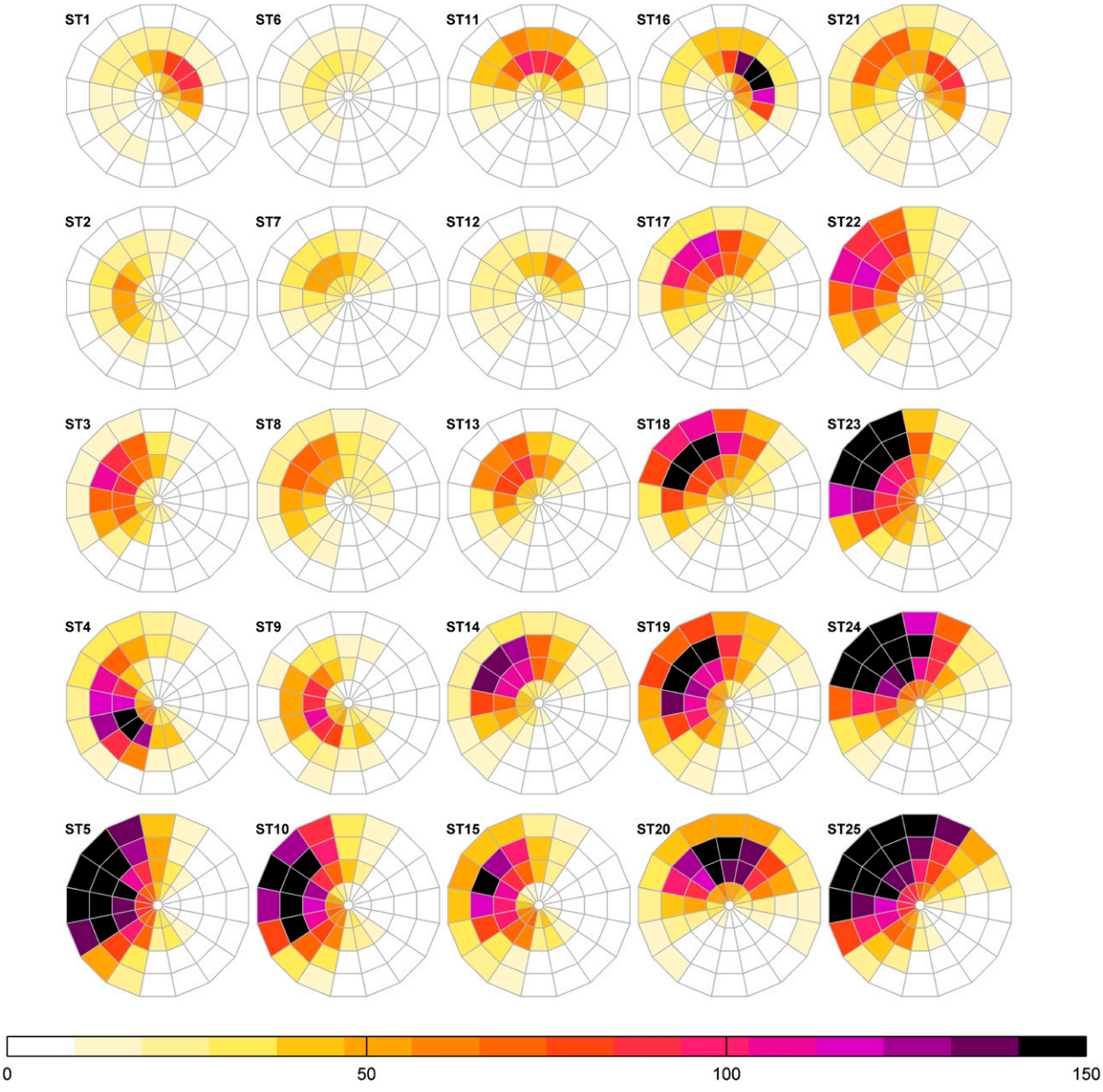

FIG. 5. Spectral-type lattice determined with the daily wave spectra (cm) from the Villano buoy record (1998–2009).

smooth the most extreme wave conditions. Nevertheless, when more wave data are available, it is possible to increase the number of clusters and to improve the extreme wave climate characterization (see Izaguirre et al. 2012).

d. Validation

In this section, the monthly moving average H_s is determined from the original data and compared with the reconstruction using the statistical spectral approach. As can be seen in Fig. 8, both series show a similar behavior at a monthly time scale, reproducing satisfactorily most of the stormy periods registered by the buoys and correctly reflecting seasonal to interannual variations. To assess the ability of the method to refill gaps several error statistics have been determined (see Fig. 8): the slope of the best linear fit b, Pearson's correlation ρ, root-mean-square (RMS) error, bias, and scatter index (SI). The b coefficient is always very close to 1 showing that the method is able to adequately reproduce both mean and stormy conditions. The RMS indicates that the major errors in the monthly H_s reconstruction do not exceed 25 and 14 cm at Villano and Cadiz, respectively. The bias is very close to 0, showing that the method does not systematically fail. Last, the scatter index indicates low dispersion

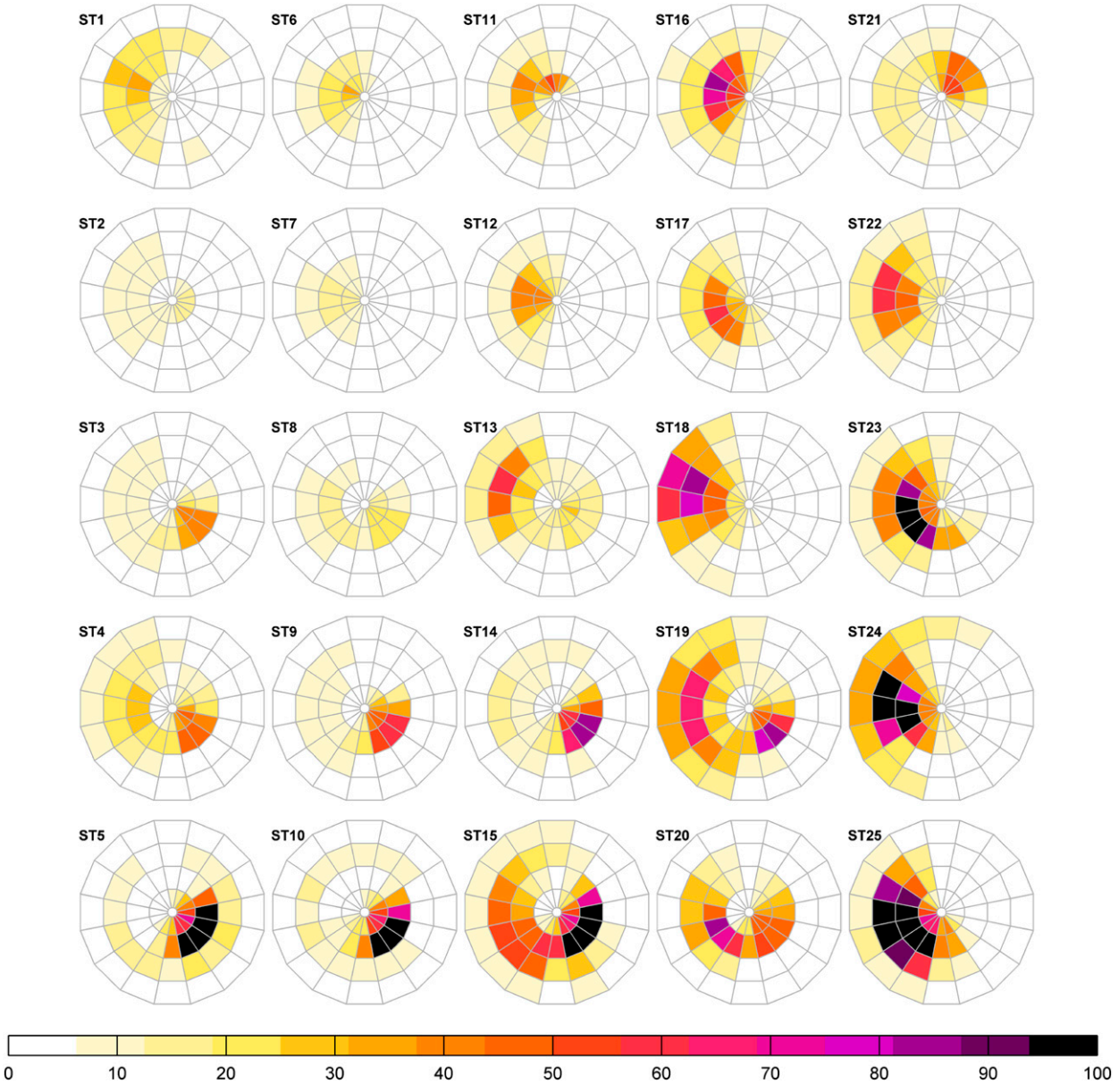

FIG. 6. As in Fig. 5, but from the Cadiz buoy record (2003–09).

of the data for H_s and T_p. Because downscaling of the wave spectra has been carried out with only 25 CTs, several discrepancies are obviously expected. This is apparent in the Cadiz buoy, in which the buoy record is not long enough. Moreover, because of the narrow configuration of the Strait of Gibraltar, and the reduced dimension of the easterly wave fetch, local atmospheric structures, which are not captured in the lattice, begin to gather importance. The assumed time 3-day lag seems to work pretty well at the more swell dominated Villano site. Meanwhile, at Cadiz the 3-day time lag looks to be appropriate for the westerly swells but not for the easterly extreme events. Additionally, we have compared the obtained wave spectra with the spectra from the Interim European Centre for Medium-Range Weather Forecasts (ECMWF) Re-Analysis (ERA-Interim) wave reanalysis (Dee et al. 2011) in terms of the annual and seasonal averages (not shown here). Quantitatively, we found that for the Villano location, which is well represented by ERA-Interim, both climatologies match quite well, with the exception that the low-frequency energy is slightly larger in the reanalysis (J. R. Bidlot 2014, personal communication). At the same time, we found that for the Cadiz location, global reanalyses might present some

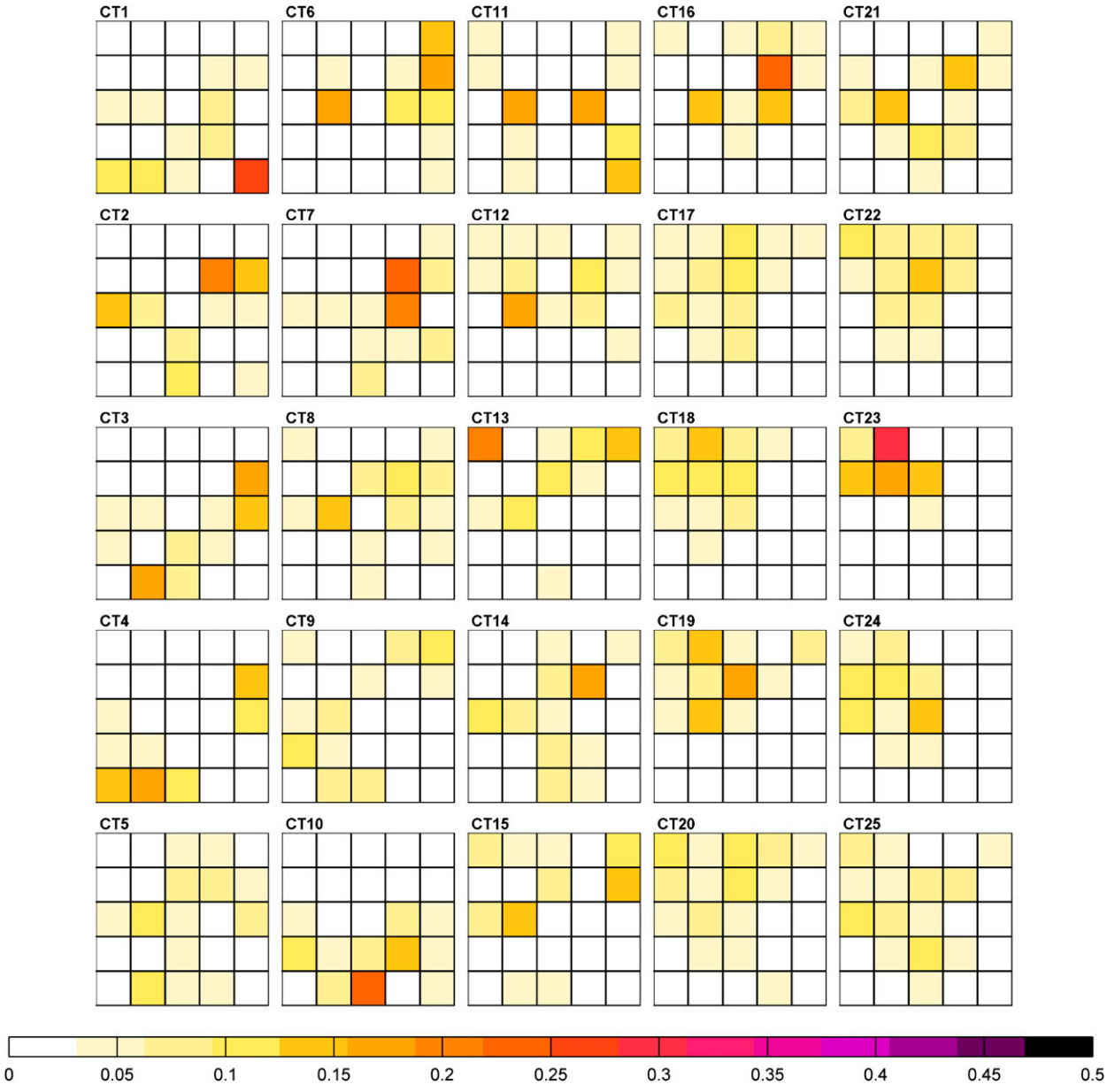

FIG. 7. Occurrence probabilities of the Villano STs projected into the WT lattice.

important deficiencies resulting from the coarse resolution. Our method can be used in these cases without the need of rerunning costly reanalyses at a finer resolution.

A key overall finding of the validation is the great ability of the statistical downscaling to refill gaps in instrumental wave records, obtaining longer and more homogeneous time series needed for climate variability studies.

4. Results

Once the daily spectra have been reconstructed during the atmospheric reanalysis temporal domain, wave climate variability is analyzed covering seasonal, interannual, and long-term trends time scales based on daily SLP fields from the CFSR reanalysis. Figure 9 displays the mean annual wave spectrum at the two locations and corresponding seasonal anomalies. As can be seen, the Villano mean spectrum exhibits a clear energy peak in the WNW sector and periods between 10 and 15 s ($\overline{h} = 65$ cm), with a significant amount of energy surrounding this bin with a small displacement toward the NW and north-northwest (NNW) directions. As expected, seasonal positive anomalies are more prominent during winter (more than 20 cm on periods

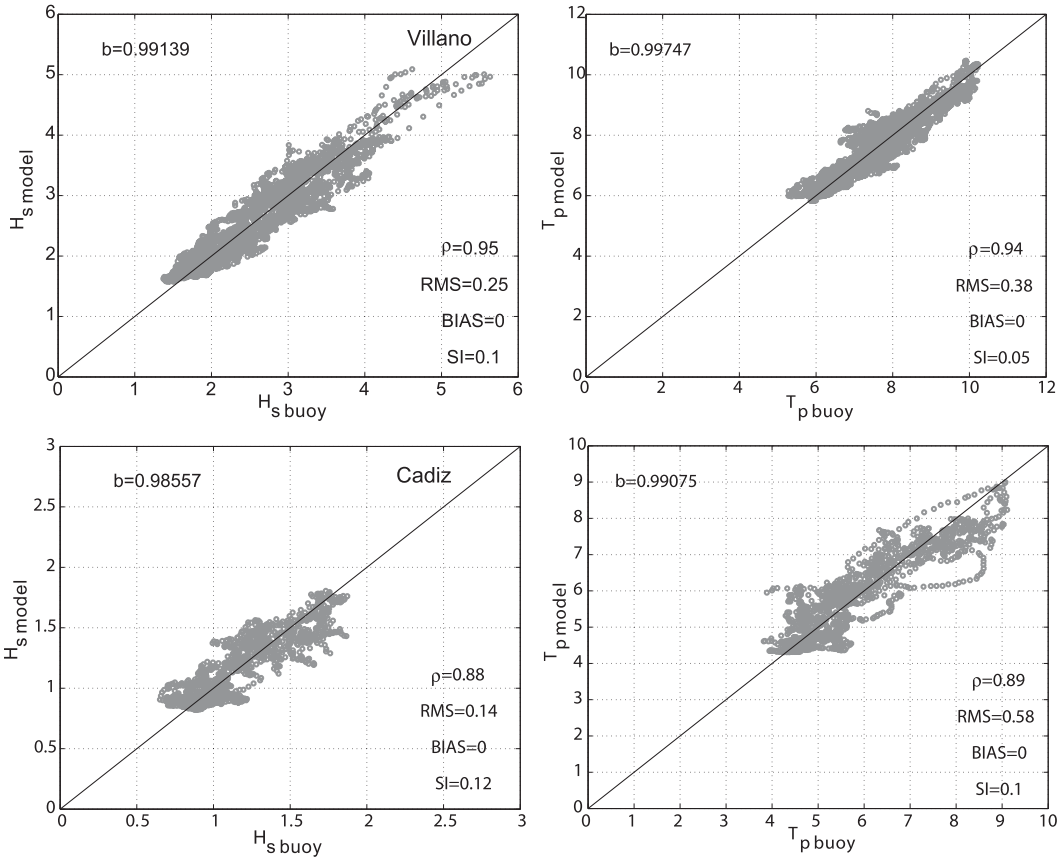

FIG. 8. Scatterplots of the monthly average (left) H_s and (right) T_p from buoys and reconstructed with the model at (top) Villano and (bottom) Cadiz. The number of data pairs is 2573 and 1576, respectively.

over 10 s in the WNW–NNW directional sector), while generalized negative anomalies take place in summer, reflecting the seasonal fluctuation of the atmosphere circulation in the NA (see Semedo et al. 2011). Spring negative anomalies on the fourth quadrant long periods reflect the small probability of the occurrence of extreme storm events during this season compared to winter. A smooth positive anomaly in the NE short periods ($\Delta h = 5$ cm) reflects the NA ridge dominance that occurs during the spring months. Fall months exhibit positive anomalies in the fourth quadrant intermediate periods due to the moderate stormy events announcing the winter period. Farther south, the Cadiz wave climate presents two clearly differentiable energy peaks: one in the SW–WNW sector and another in the SE. The wave climate in this region is not as severe as at Villano; consequently, much less energy is found in the longest periods. Again, seasonal anomalies are stronger in winter responding to the major SLP gradients in this season.

As was said before, there is not a unique manifestation of the wave climate variability of one climate index. With the nonlinear clustering techniques, it is easy to determine occurrence probabilities of each selected ST depending on the value of the climate index. Nevertheless, in order to analyze the relationship of the wave climate to universally accepted climate patterns such as the NAO (Barnston and Livezey 1987), it seems insightful to proceed with the linear approach, calculating correlation values of the monthly standardized wave height anomalies of the most prominent climate indices governing the climate in the NA. Figure 10 shows the correlation values of the wave spectra and AO (Thompson and Wallace 1998), NAO, and the east Atlantic index (EA; Barnston and Livezey 1987). Significant values at the 95% confidence interval are dotted. The AO and the NAO indices have been taken as the dominant modes of the Northern Hemisphere and the NA climate variability, respectively. The EA index has been chosen as a more local predictor of the atmosphere circulation over the eastern part of the NA. As can be observed, major correlation values are found with the most local climate index. The positive phases of EA, characterized by low pressures southwest of the British

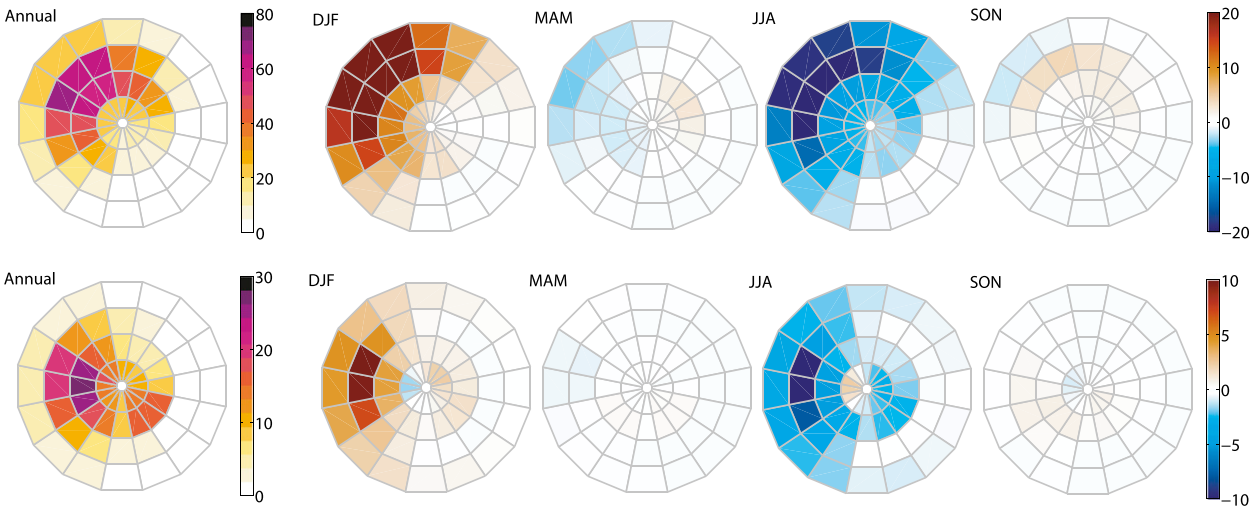

FIG. 9. Mean annual wave spectrum and seasonal anomalies (cm) from the statistical model (1979–2009) at (top) Villano and (bottom) Cadiz.

Isles correlates positively ($\beta > 0.4$) with the energy composed in all the frequency bands of the third directional sector, reflecting the strong southwesterly winds blowing directly over the Villano buoy location (Charles et al. 2012). At Cadiz, waves generated during active phases of the AO tend to reach the target point with a strong decay in the short periods. Comparing the effect of the AO and NAO on waves, it is important to remark that the index correlation spectral patterns are similar for both climate indices at Villano, while some nuances appear at Cadiz. While the AO seems to be more related with the zonal migration of the storm tracks, farther to the north during +AO and farther to the south during −AO (see upper-left panel), at Cadiz there is an east–west shift of the wave field dominance, while at Villano the oscillation is north–south. Regarding the NAO, a western migration of the positive anomalies is observed at Villano when comparing it with the AO. On the other hand at Cadiz, the reinforcing of the high pressure systems during positive phases of the NAO is observed in the positive correlation appearing in the ENE short periods. Significant positive correlation also appears in the WNW intermediate periods. These results agree with the recent works of Charles et al. (2012) and Le Cozannet et al. (2011) in which they argue that in the Bay of Biscay larger waves and periods propagate from the NNW during +NAO and from the W during +EA.

Last, in Fig. 11 seasonal long-term trends are displayed. Although the rates of change are smoothed by the downscaling technique, these results provide a qualitative representation of the general picture of changes in the frequency–direction wave energy distribution throughout the 31-yr period. In agreement with previous works (Wang and Swail 2001; Wang and Swail 2002; Woolf et al. 2002; Dupuis et al. 2006; Semedo et al. 2011), no significant trend has been obtained for the annual-mean H_s in the Bay of Biscay. Similar to Charles et al. (2012), we only found significant summer trends at both locations. The spectral pattern of the summer trend is quite similar in both sites, exhibiting an increase of the short-period waves from the west and a decrease of the easterly seas.

5. Conclusions

In this study an analysis of the spectral wave climate in the east NA has been presented. The work is based on the combination of measured wave data from two deep-water buoys and the CFSR atmospheric reanalysis that, by means of clustering statistical methods, allows for the reconstruction of the daily wave spectra throughout the entire hindcast time coverage. Moreover, the proposed method facilitates the establishment of direct relationships between atmospheric synoptic states and the most common spectral wave conditions at the target locations. Rather than working with the SLP produced by the atmospheric model, the synoptic atmospheric clustering has been conducted for the 3-day-averaged squared SLP gradients, emphasizing the wind direction and the configuration of the surface wind jets over the NA. The 25 circulation types have been determined with the principal component time series from the EOF decomposition. It has been shown that even with a low number of clusters, a wide range of atmospheric situations are captured, differentiating between some important

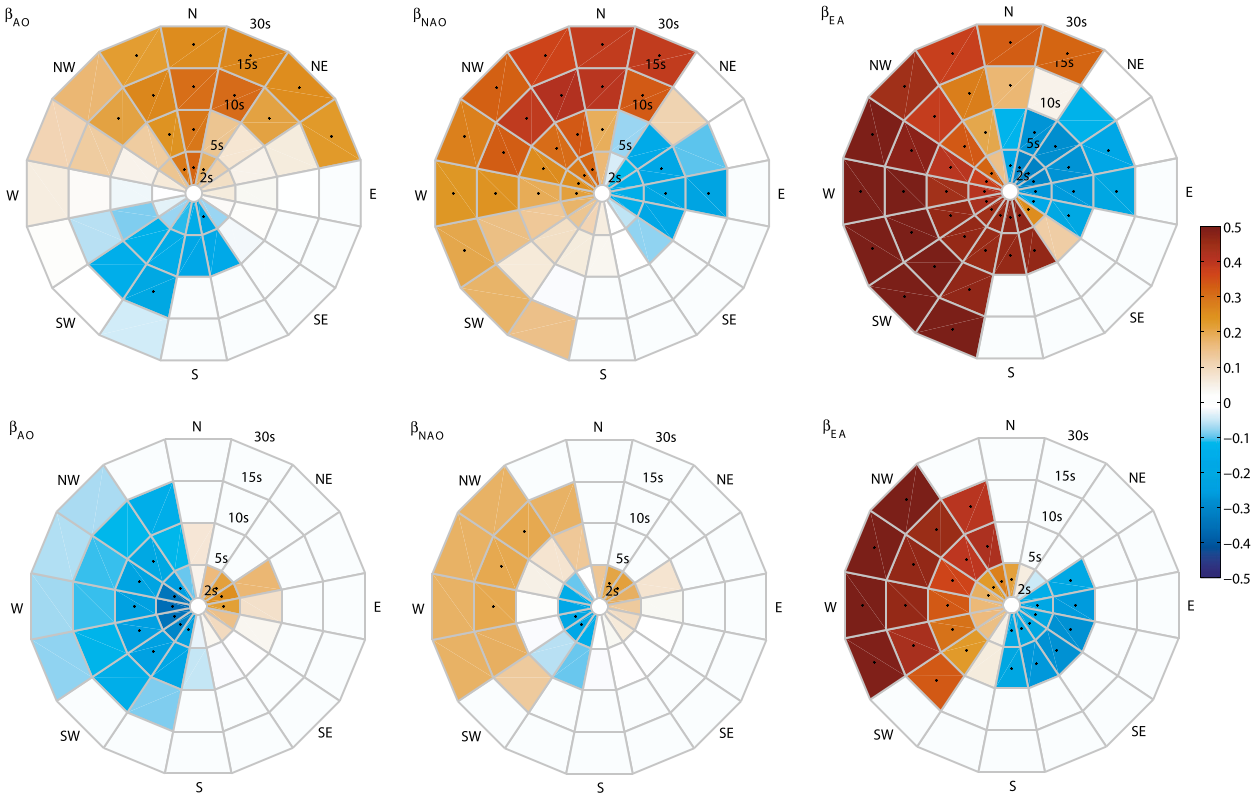

FIG. 10. Correlation values of the wave spectra with the AO, NAO, and EA climate indices, (top) Villano and (bottom) Cadiz, significant values at the 95% confidence interval are dotted.

nuances with dramatic effects on the wave generation processes.

The same procedure has been followed to obtain the most recurrent daily wave spectra at the two studied sites. First, the directional full spectra have been discretized in a reduced number of bins to make the information more easily understandable. Again, the *k*-means algorithm has shown excellent skill when working with wave spectra. Moreover, the 25 identified spectral types at each site provide considerably more information about the wave conditions than the traditionally used aggregated or statistical wave parameters. Wave sources can be sensed when visually inspecting the discrete spectrum by allowing some differentiation between the strength and the position of the ocean storms.

The occurrence probabilities of the selected spectral types have been determined for each identified circulation type, obtaining multigrid maps linking the wave spectra with the synoptic atmospheric patterns. This crossed information allows for the identification of the most unfavorable atmospheric situations able to generate extreme or anomalous sea states and facilitates the understanding of the physical principles of wave generation and deep-ocean propagation. Moreover, by means of this technique, 31 years of daily directional wave spectra at the target points have been obtained. The generation of long and homogeneous time series contributes to overcoming the most limiting requirement when studying wave climate variability. Thus, seasonal, interannual, and long-term trends have been investigated. Seasonal variations of the discrete wave spectra capture the Iceland low and Azores high winter–summer dominance. Furthermore, seasonal anomalies reveal important details of the frequency–direction wave energy distribution throughout the year. Interannual variations of the spectral wave climate have been explored by considering linear relationships of the monthly standardized anomalies of the energy within each bin of the discrete spectrum with respect to well-known climate indices governing the climate variability of the NA. Results disclose more aspects than traditional approaches based on aggregated or statistical wave parameters, as, for example, specifying frequencies and directions in which the analyzed climate pattern has significant effects.

Last, the spectral long-term trends of the east NA analysis have been evaluated on a seasonal basis. Results show increased summer medium-period westerly

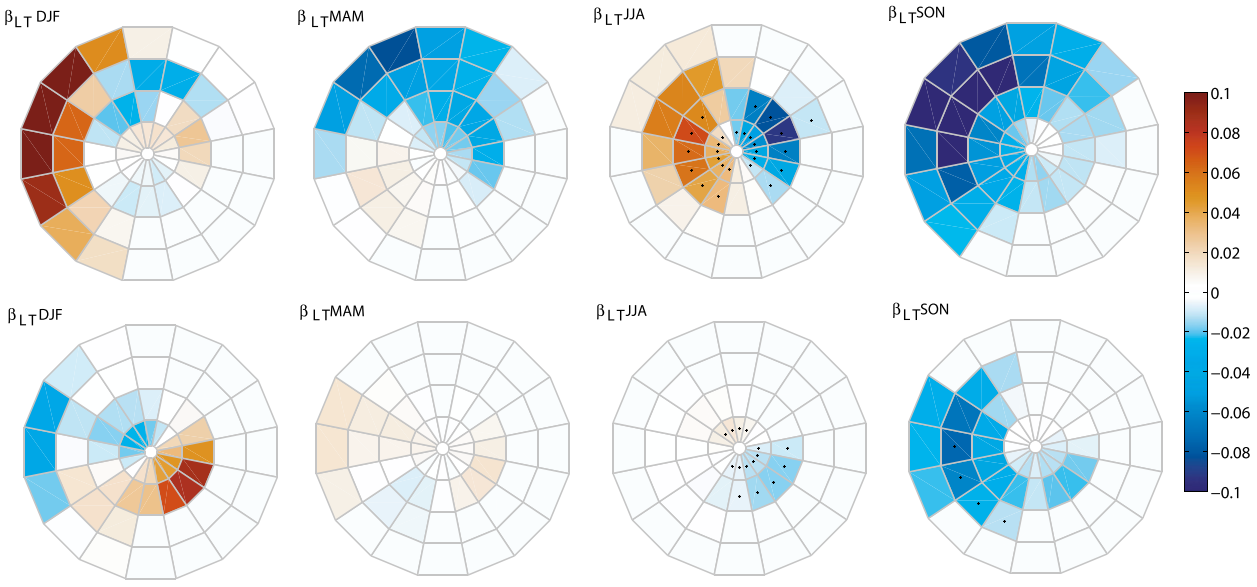

FIG. 11. Seasonal linear trends (cm yr^{-1}) of the discrete wave spectra from 1979 to 2009, (top) Villano and (bottom) Cadiz; significant values at the 95% confidence interval are dotted.

energy at Villano and a decrease of the easterly short-period waves at both locations. No significant trends have been found in other seasons.

The simple applicability of the circulation-type framework provides a useful descriptive graphical tool that helps to understand the effect of the atmospheric circulation pattern on the directional wave spectra. Going further, the application described in this paper allows for the study of climate variability over a wide range of time scales, from days to the exploration of wave climate projections for different Intergovernmental Panel on Climate Change (IPCC) scenarios from global circulation models runs.

Acknowledgments. The authors are grateful to Puertos del Estado (Spanish Ministry of Public Works and Infrastructures) for providing us the instrumental buoy data. This work was partially funded by the project IMAR21 (CT M2010-15009) from the Spanish Government. We thank Jean-Raymond Bidlot for his constructive comments and for providing the ERA-Interim spectral data.

REFERENCES

Alves, J., 2006: Numerical modeling of ocean swell contributions to the global wind-wave climate. *Ocean Modell.,* **11,** 98–122, doi:10.1016/j.ocemod.2004.11.007.

Barnston, A. G., and R. E. Livezey, 1987: Classification, seasonality and persistence of low-frequency atmospheric circulation patterns. *Mon. Wea. Rev.,* **115,** 1083–1126, doi:10.1175/1520-0493(1987)115<1083:CSAPOL>2.0.CO;2.

Barry, R. G., and A. H. Perry, 1973: *Synoptic Climatology: Methods and Applications.* Methuen, 555 pp.

Bromirski, P. D., D. R. Cayan, and R. E. Flick, 2005: Wave spectral energy variability in the northeast Pacific. *J. Geophys. Res.,* **110,** C03005, doi:10.1029/2004JC002398.

Caires, S., V. R. Swail, and X. L. Wang, 2006: Projection and analysis of extreme wave climate. *J. Climate,* **19,** 5581–5605, doi:10.1175/JCLI3918.1.

Camus, P., F. J. Mendez, and R. Medina, 2011a: A hybrid efficient method to downscale wave climate to coastal areas. *Coastal Eng.,* **58,** 851–862, doi:10.1016/j.coastaleng.2011.05.007.

——, ——, ——, and A. S. Cofiño, 2011b: Analysis of clustering and selection algorithms for the study of multivariate wave climate. *Coastal Eng.,* **58,** 453–462, doi:10.1016/j.coastaleng.2011.02.003.

Cassou, C., L. Terray, J. W. Hurrell, and C. Deser, 2004: North Atlantic winter climate regimes: Spatial asymmetry, stationarity with time, and oceanic forcing. *J. Climate,* **17,** 1055–1068, doi:10.1175/1520-0442(2004)017<1055:NAWCRS>2.0.CO;2.

Cavazos, T., 2000: Using self-organizing maps to investigate extreme climate events: An application to wintertime precipitation in the Balkans. *J. Climate,* **13,** 1718–1732, doi:10.1175/1520-0442(2000)013<1718:USOMTI>2.0.CO;2.

Charles, E., D. Idier, J. Thiébot, G. Le Cozannet, R. Pedreros, F. Ardhuin, and S. Planton, 2012: Present wave climate in the Bay of Biscay: Spatiotemporal variability and trends from 1958 to 2001. *J. Climate,* **25,** 2020–2039, doi:10.1175/JCLI-D-11-00086.1.

Dee, D. P., and Coauthors, 2011: The ERA-Interim Reanalysis: Configuration and performance of the data assimilation system. *Quart. J. Roy. Meteor. Soc.,* **137,** 553–597, doi:10.1002/qj.828.

Dupuis, H., D. Michel, and A. Sottolichio, 2006: Wave climate evolution in the Bay of Biscay over two decades. *J. Mar. Syst.,* **63,** 105–114, doi:10.1016/j.jmarsys.2006.05.009.

Gerling, T. W., 1992: Partitioning sequences and arrays of directional spectra into component wave systems. *J. Atmos. Oceanic*

Technol., **9,** 444–458, doi:10.1175/1520-0426(1992)009<0444:PSAAOD>2.0.CO;2.

Gutierrez, J. M., R. Cano, A. S. Cofiño, and C. Sordo, 2005: Analysis and downscaling multi-model seasonal forecast in Peru using self-organizing maps. *Tellus,* **57A,** 435–447, doi:10.1111/j.1600-0870.2005.00128.x.

Hastie, T., R. Tibshirani, and J. Friedman, 2001: *The Elements of Statistical Learning: Data Mining, Inference, and Prediction.* Springer, 533 pp.

Hurrell, J. W., and C. Deser, 2009: North Atlantic climate variability: The role of the North Atlantic Oscillation. *J. Mar. Syst.,* **78,** 28–41, doi:10.1016/j.jmarsys.2008.11.026.

Izaguirre, C., M. Menendez, P. Camus, F. J. Mendez, R. Minguez, and I. J. Losada, 2012: Exploring interannual variability of the extreme wave climate in the northeast Atlantic Ocean. *Ocean Modell.,* **59–60,** 31–40, doi:10.1016/j.ocemod.2012.09.007.

Janssen, P. A. E. M., and P. Viterbo, 1996: Ocean waves and the atmospheric climate. *J. Climate,* **9,** 1269–1287, doi:10.1175/1520-0442(1996)009<1269:OWATAC>2.0.CO;2.

Le Cozannet, G., S. Lecacheux, E. Delvallee, N. Desramaut, C. Oliveros, and R. Pedreros, 2011: Teleconnection pattern influence on sea-wave climate in the Bay of Biscay. *J. Climate,* **24,** 641–652, doi:10.1175/2010JCLI3589.1.

Preisendorfer, R. W., 1988: *Principal Component Analysis in Meteorology and Oceanography.* C. D. Mobley, Ed., Elsevier, 401 pp.

Saha, S., and Coauthors, 2010: The NCEP Climate Forecast System Reanalysis. *Bull. Amer. Meteor. Soc.,* **91,** 1015–1057, doi:10.1175/2010BAMS3001.1.

Semedo, A., S. K. Rutgersson, and A. Sterl, 2011: A global view on the wind sea and swell climate and variability from ERA-40. *J. Climate,* **24,** 1461–1479, doi:10.1175/2010JCLI3718.1.

Thompson, D. W. J., and J. M. Wallace, 1998: The Arctic Oscillation signature in the wintertime geopotential height and temperature fields. *Geophys. Res. Lett.,* **25,** 1297–1300, doi:10.1029/98GL00950.

Wang, D. W., and P. A. Hwang, 2001: An operational method for separating wind sea and swell from ocean wave spectra. *J. Atmos. Oceanic Technol.,* **18,** 2052–2062, doi:10.1175/1520-0426(2001)018<2052:AOMFSW>2.0.CO;2.

Wang, X. L., and V. R. Swail, 2001: Changes in extreme wave heights in Northern Hemisphere oceans and related atmospheric circulation regimes. *J. Climate,* **14,** 2204–2221, doi:10.1175/1520-0442(2001)014<2204:COEWHI>2.0.CO;2.

——, and ——, 2002: Trends of Atlantic wave extremes as simulated in a 40-yr wave hindcast using kinematically reanalyzed wind fields. *J. Climate,* **15,** 1020–1035, doi:10.1175/1520-0442(2002)015<1020:TOAWEA>2.0.CO;2.

——, and ——, 2006: Climatology and changes of extratropical cyclone activity: Comparison of ERA-40 with NCEP–NCAR reanalysis for 1958–2001. *J. Climate,* **19,** 3145–3166, doi:10.1175/JCLI3781.1.

——, Y. Feng, and V. R. Swail, 2012: North Atlantic wave height trends as reconstructed from the 20th century reanalysis. *Geophys. Res. Lett.,* **39,** L18705, doi:10.1029/2012GL053381.

Woolf, D. K., P. G. Challenor, and P. D. Cotton, 2002: Variability and predictability of the North Atlantic wave climate. *J. Geophys. Res.,* **107,** 3145, doi:10.1029/2001JC001124.